INTERNATIONAL JOURNAL FOR NUMERICAL AND ANALYTICAL METHODS IN GEOMECHANICS
Int. J. Numer. Anal. Meth. Geomech., 2002; **26**:499–513 (DOI: 10.1002/nag.209)

A fractal comminution approach to evaluate the drilling energy dissipation

Alberto Carpinteri*,† and Nicola Pugno‡

Department of Structural Engineering and Geotechnics, Politecnico di Torino, Corso Duca degli Abruzzi 24, 10129 Torino, Italy

SUMMARY

The drilling comminution is theoretically and experimentally analysed by a fractal approach. An extension of the Third Comminution Theory is developed to evaluate the energy dissipation in the process: it occurs in a fractal domain intermediate between a surface and a volume. The theoretical assumption of a material 'quantum' is experimentally observed. The experimental fragment analysis evidences the characteristic size of separation between primary cutting and secondary milling. A global power balance for the drilling process is also presented and permits the prediction of drilling velocity. It shows also how the dissipation energy density (drilling strength) is not a constant parameter, but decreases considerably with the size scale. Copyright © 2002 John Wiley & Sons, Ltd.

1. INTRODUCTION

Fragmentation and comminution [1] play an important role in a variety of phenomena, both natural and man-made. Star explosion and meteor impact are examples of natural processes producing fragmented ejecta. Although fragmentation is of considerable importance and many experimental, numerical and theoretical studies have been carried out, relatively little progress has been made till now in developing related comprehensive theories. Fragmentation involves the interaction between fractures over a wide range of scales and a fractal fragment size distribution is expected [2].

Fractals are hierarchical, often highly irregular, and self-similar objects [3,4]. As a result, no matter how complex a particular spatial pattern might be, the statistical properties of this pattern can be reproduced at different length scales. Such scale-invariant systems offer new opportunities for modelling the propagation of multiple fractures at different length scales.

*Correspondence to: Alberto Carpinteri, Department of Structural Engineering and Geotechnics, Politecnico di Torino, Corso Duca degli Abruzzi 24, 10129 Torino, Italy.
†E-mail: carpinteri@polito.it
‡E-mail: pugno@polito.it

Contract/grant sponsor: Ministry of University and Scientific Research (MIUR)
Contract/grant sponsor: National Research Council (CNR)
Contract/grant sponsor: EC-TMR; Contract/grant number: ERBFMRXCT960062

Received 6 July 2001
Revised 19 November 2001

Because of their complexity at any given scale, they are particularly applicable to heterogeneous materials.

Fragmentation can occur as a result of dynamic crack propagation during compressive/tensile loading (dynamic fragmentation) or due to stress waves and their reflections during impact loading (ballistic fragmentation). These processes have been reviewed in References [5–8]. A review on drilling indentation and the physical mechanisms of hard rock fragmentation under mechanical loading has been performed in Reference [9]; an experimental analysis of the variation of drilling detritus with operating parameters has been reported in Reference [10].

Several theoretical models have been proposed linking fractals to fracture and fragmentation. Carpinteri [11] and Carpinteri *et al*. [12,13] used the fractal and multifractal approaches to explain the scaling laws for strength and toughness in the breaking behaviour of disordered materials. Engleman *et al*. [14] applied the maximum entropy method to show that the number-size distribution follows a fractal law for fragments that are not too large. By combining a fractal analysis of brittle fracture with energy balance principles, a theoretical expression for the fragment size distribution is derived as a function of energy density [15,16]. In Reference [17] the fragment size distribution is predicted from clusters of connected bonds in a cubic lattice using percolation theory. A suite of fractal models has been developed in References [8,18–22]; these authors use the probabilities of failure to predict the fragment-size distribution from the knowledge of the geometrical properties of the original material.

More recently, fragmentation has been studied from physical [23–25] and geophysical [26–28] points of view, for compression [29–31] and impact [32–35] phenomena, as well as for comminution technologies [36,37].

2. ENERGY DISSIPATED IN THE COMMINUTION PROCESS

After comminution or fragmentation, the *cumulative distribution* of particles with radius smaller than r is

$$P(<r) = 1 - \left(\frac{r_{\min}}{r}\right)^D \tag{1}$$

where experimentally it is typically $2<D<3$ [2]. The related boundary conditions are:

$$P(<r_{\min}) = 0 \tag{2a}$$

$$P(<r_{\max}) \cong 1 \tag{2b}$$

if $r_{\min} \ll r_{\max}$.

Of course, the complementary cumulative distribution of particles with radius larger than r is

$$P(>r) = 1 - P(<r) = \left(\frac{r_{\min}}{r}\right)^D \tag{3}$$

The *probability density function* $p(r)$ multiplied by the interval amplitude $\mathrm{d}r$ represents the fraction of particles with radius intermediate between r and $r + \mathrm{d}r$. It is provided by derivation of the cumulative distribution function (1):

$$p(r) = \frac{\mathrm{d}P(<r)}{\mathrm{d}r} = D\,\frac{r_{\min}^D}{r^{D+1}} \tag{4}$$

The total fracture surface area is obtained by integration:

$$A = \int_{r_{\min}}^{r_{\max}} N_{\mathrm{p}}(4\pi r^2)p(r)\,\mathrm{d}r \tag{5}$$

where N_{p} is the total number of particles.

Introducing Equation (4) into Equation (5) we obtain:

$$\begin{aligned} A &= 4\pi N_{\mathrm{p}} \frac{D}{D-2} r_{\min}^{D} \left(\frac{1}{r_{\min}^{D-2}} - \frac{1}{r_{\max}^{D-2}} \right) \\ &\cong 4\pi N_{\mathrm{p}} \frac{D}{D-2} r_{\min}^{2} \end{aligned} \tag{6}$$

On the other hand, the total volume of the particles is

$$\begin{aligned} V &= \int_{r_{\min}}^{r_{\max}} N_{\mathrm{p}} \left(\frac{4}{3}\pi r^3 \right) p(r)\,\mathrm{d}r \\ &= \frac{4}{3}\pi N_{\mathrm{p}} \frac{D}{3-D} r_{\min}^{D} (r_{\max}^{3-D} - r_{\min}^{3-D}) \cong \frac{4}{3}\pi N_{\mathrm{p}} \frac{D}{3-D} r_{\min}^{D} r_{\max}^{3-D} \end{aligned} \tag{7}$$

If we assume a material 'quantum' of size $r_{\min} = \text{constant}$ [26,38,39], and a hypothesis of self-similarity, i.e., $r_{\max} = \bar{k}\sqrt[3]{V}$, $\bar{k} = \text{constant}$ [40], the energy dissipated to produce the new free surface in the comminution process, which is provided by the product of fracture energy $\mathscr{G}_{\mathrm{F}}$ and total fracture surface area $A/2$ [41,42] ($A/2$ and not A because it is in common between fragments), is

$$\begin{aligned} W &= \frac{1}{2}\mathscr{G}_{\mathrm{F}} A = \mathscr{G}_{\mathrm{F}} V \left(\frac{3}{2} \frac{3-D}{D-2} r_{\min}^{2-D} r_{\max}^{D-3} \right) \\ &= \frac{3}{2} \frac{3-D}{D-2} \frac{\mathscr{G}_{\mathrm{F}}}{r_{\min}^{D-2} \bar{k}^{3-D}} V^{D/3} = \mathscr{G}_{\mathrm{F}}^{*} V^{D/3} \end{aligned} \tag{8}$$

and represents an extension of the Third Comminution Theory, where $W \propto V^{2.5/3}$ [43].

The extreme cases contemplated by Equation (8) are represented by $D = 2$, surface theory [44,45], when the dissipation really occurs on a surface ($W \propto V^{2/3}$), and by $D = 3$, volume theory [45,46], when the dissipation occurs in a volume ($W \propto V$). The experimental cases of comminution are usually intermediate ($D \cong 2.5$), as well as the size distribution for concrete aggregates due to Füller [47]. On the other hand, concrete aggregates frequently are a product of natural fragmentation or artificial comminution. If the material to be fragmented is concrete, we have therefore a double reason to expect $D \cong 2.5$.

The energy dissipation occurs on a two-dimensional surface according to Griffith, rather than on a morphologically fractal set. On the other hand, the distribution of particle size follows a power-law, the number of infinitesimal particles tending to infinity.

3. MATERIAL 'QUANTUM' AND SELF-SIMILARITY ASSUMPTIONS

The fundamental assumptions of material 'quantum' and of self-similarity can be derived from the more general hypothesis that the energy dissipation must occur in a fractal domain intermediate, in any case, between a surface and a volume.

If we assume $D<2$, from Equation (6) we have

$$A \cong 4\pi N_{\mathrm{p}} \frac{D}{2-D} r_{\min}^{D} r_{\max}^{2-D} \tag{9}$$

Equation (7) is still valid and then Equation (8) becomes

$$W = \frac{1}{2}\mathscr{G}_{\mathrm{F}} A = \frac{3}{2}\frac{3-D}{2-D}\frac{\mathscr{G}_{\mathrm{F}}}{r_{\max}} V \tag{10}$$

From Equation (10) we obtain $r_{\max} = \bar{k}\sqrt[3]{V}$, if the dissipation is assumed to be proportional to $V^{2/3}$ even when $D<2$.

If we assume $D>3$, from Equation (7) we have

$$V \cong \frac{4}{3}\pi N_{\mathrm{p}} \frac{D}{D-3} r_{\min}^{3} \tag{11}$$

Equation (6) is still valid and then Equation (8) becomes

$$W = \frac{1}{2}\mathscr{G}_{\mathrm{F}} A = \frac{3}{2}\frac{D-3}{D-2}\frac{\mathscr{G}_{\mathrm{F}}}{r_{\min}} V \tag{12}$$

From Equation (12) we obtain $r_{\min} = \text{constant}$, if the dissipation is assumed to be proportional to V even when $D>3$.

Usually, from comminution experiments [3] we get $2<D<3$ and only infrequently values do not belong to such interval, so that the energy dissipation will occur in a fractal domain intermediate between a surface and a volume. On the other hand, in the latter cases the physical meaning is clear, as the dissipation occurs in a surface ($D<2$) or in a volume ($D>3$).

4. EXPERIMENTAL FRACTAL ASSESSMENT: THE SINGLE-SCRATCH TEST

Equation (7) can be utilized to compute the mass of the particles with radius smaller than r:

$$M(<r) \cong \frac{4}{3}\pi N_{\mathrm{p}} \rho_m \frac{D}{3-D} r_{\min}^{D} r^{3-D} \tag{13}$$

where ρ_m is the material density, so that the ratio of this partial mass to the total mass is

$$\frac{M(<r)}{M} \cong \left(\frac{r}{r_{\max}}\right)^{3-D} \tag{14}$$

The logarithmic version of Equation (14) becomes

$$\log\frac{M(<r)}{M} = (3-D)\log\frac{r}{r_{\max}} \tag{15}$$

Equation (15) represents a straight line passing through the origin in the bilogarithmic plane, i.e. a fractal law, with slope equal to $3-D$. An *ad hoc* experiment on a single-scratch test has been performed by a laser diffraction sensor HELOS. This system is the first for which the

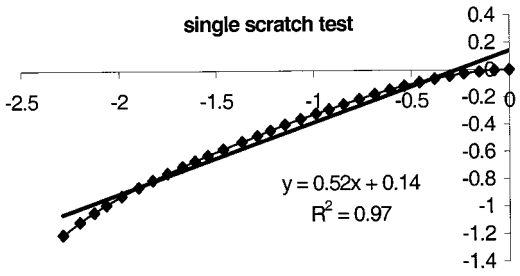

Figure 1. Bi-logarithmic diagrams of relative size x vs relative mass y of fragments (experimental points and theoretical straight line).

Fraunhofer method is applied over the whole measuring range from 0.1 to 8750 μm. It is the classical instrument for dry and wet particle size analysis of powders, suspensions, emulsions or sprays. The results obtained for the detritus size distribution are shown in Figure 1, where $x = \log(r/r_{\max})$ and $y = \log M(<r)/M$.

As predicted, the trend is substantially linear with a fractal exponent $D = 2.48$.

5. EXPERIMENTS ON DRILLING COMMINUTION

Some experiments of conventional drilling perforation on concrete have been performed. The operating parameters are reported in Section 6. The drilling detritus, removed by a refrigerant water flow (5×10^{-5} m^3/s), has been analysed by the laser diffraction sensor HELOS, which has permitted to obtain the size distribution of the fragments. The results obtained are reported in Figures 2–7, where horizontal axis is $x = \log(r/r_{\max})$ and vertical axis is $y = \log M(<r)/M$.

The global trend moves away from linearity (see the first diagrams at the top of each page). On the other hand, the substantial bilinearity of the global diagrams emphasizes the presence of two distinct comminution mechanisms: (1) *cutting*, with the formation of the larger chips; (2) *milling*, with the formation of the smaller particles. This analysis presents the advantage of separating the two effects (see the second and third diagrams from the top of each page), without additional experiments, and of providing the fractal exponents D_{I} and D_{II} for, respectively, primary and secondary comminutions:

Sample 1: $D = 2.67$, $D_{\mathrm{I}} = 2.87$, $D_{\mathrm{II}} = 2.08$
Sample 2: $D = 2.67$, $D_{\mathrm{I}} = 2.88$, $D_{\mathrm{II}} = 2.08$
Sample 3: $D = 2.78$, $D_{\mathrm{I}} = 2.85$, $D_{\mathrm{II}} = 2.40$
Sample 4: $D = 2.76$, $D_{\mathrm{I}} = 2.84$, $D_{\mathrm{II}} = 2.40$
Sample 5: $D = 2.60$, $D_{\mathrm{I}} = 2.87$, $D_{\mathrm{II}} = 2.08$
Sample 6: $D = 2.58$, $D_{\mathrm{I}} = 2.84$, $D_{\mathrm{II}} = 2.04$

The primary fractal exponent D_{I} is close to 3. It means that energy dissipation for coarse chipping is substantially in the volume, as well as for finer milling it is substantially on the surface, D_{II} being close to 2 [48].

This is consistent with the classical laws of fragmentation and comminution. As a matter of fact, experimental investigations have shown that Kick's law (energy proportional to the volume, [46]) describes coarse fragmentation consistently, whereas Rittinger's law (energy

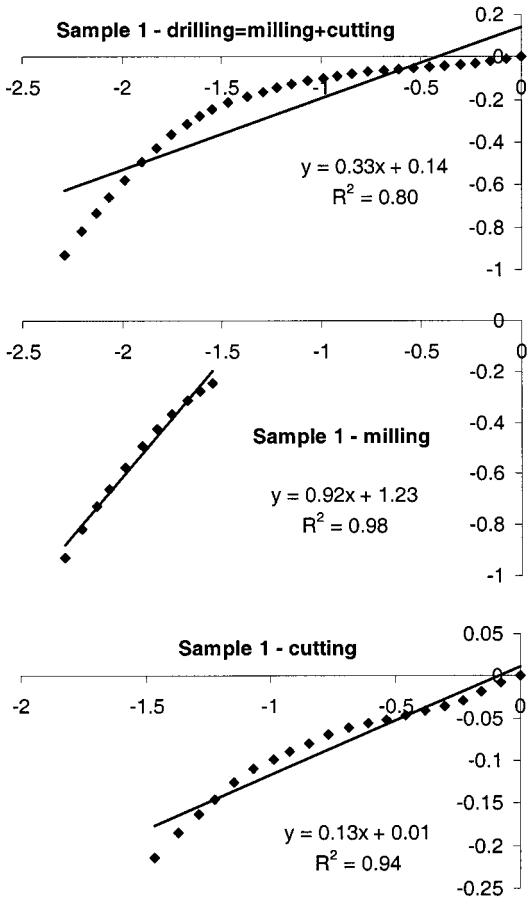

Figure 2. Sample 1—Bi-logarithmic diagrams of relative size x vs relative mass y of fragments (experimental points and theoretical curve) for drilling detritus (all particles), for milling (smaller particles) and cutting (larger particles).

proportional to the surface, [44]) is more reliable for the finer comminution. The abscissa $\bar{x}$ of separation between the two approximately linear diagrams provides the particle diameter $\bar{d} = 10^{\bar{x}} d_{\max}$, above which the fragments are produced by *cutting* and under which the particles are produced by *milling* (or crushing):

Sample 1: $\bar{x} \cong -1.5$, $d_{\max} = 350$ μm, $\bar{d} = 11$ μm
Sample 2: $\bar{x} \cong -1.5$, $d_{\max} = 350$ μm, $\bar{d} = 11$ μm
Sample 3: $\bar{x} \cong -1.5$, $d_{\max} = 365$ μm, $\bar{d} = 12$ μm
Sample 4: $\bar{x} \cong -1.5$, $d_{\max} = 365$ μm, $\bar{d} = 12$ μm
Sample 5: $\bar{x} \cong -1.3$, $d_{\max} = 246$ μm, $\bar{d} = 12$ μm
Sample 6: $\bar{x} \cong -1.3$, $d_{\max} = 206$ μm, $\bar{d} = 10$ μm

The value of the threshold size $\bar{d}$ is approximately independent of the considered sample:

$$\bar{d} \approx 10 \text{ μm} \tag{16}$$

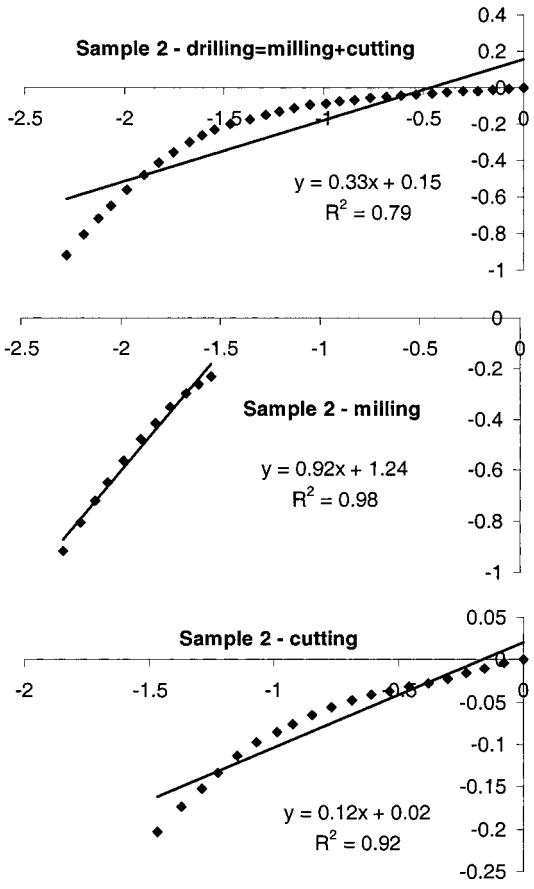

Figure 3. Sample 2—Bi-logarithmic diagrams of relative size x vs relative mass y of fragments (experimental points and theoretical curve) for drilling detritus (all particles), for milling (smaller particles) and cutting (larger particles).

From experiments the characteristic size of the material 'quantum' appears to be approximately

$$d_{\min} \cong 1\ \mu\text{m} \tag{17}$$

6. POWER BALANCE FOR DRILLING COMMINUTION

Considering the vertical thrust force F, the torque M_t and their dual displacements δ and φ, the power balance for drilling comminution can be written as

$$F\dot{\delta} + M_t\dot{\varphi} = \dot{W}_{\mathrm{I}} + \dot{W}_{\mathrm{II}} + \dot{W}_{\mathrm{f}} \tag{18}$$

where W_{I} and W_{II} represent the global work dissipated (by fracture and by internal friction) in the primary and secondary comminution processes, respectively, W_{f} is the heat production by external friction and the dot over the symbols represents time derivation [49,50].

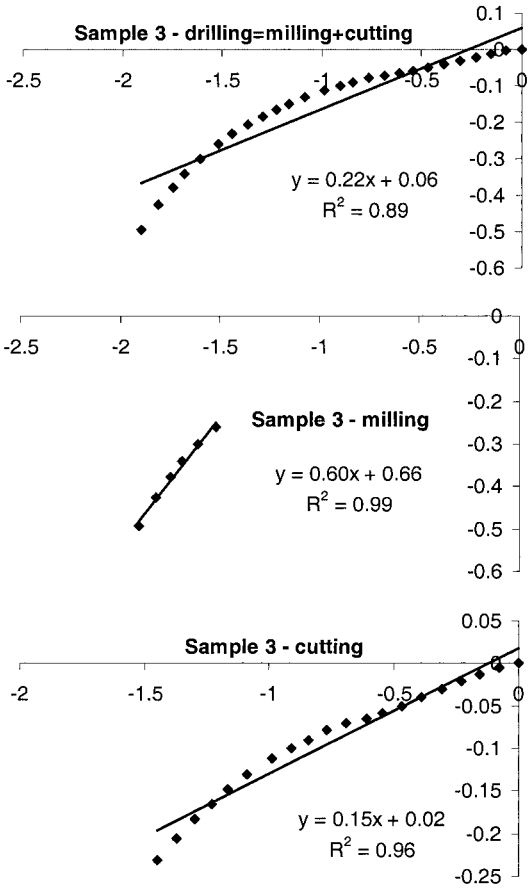

Figure 4. Sample 3—Bi-logarithmic diagrams of relative size x vs relative mass y of fragments (experimental points and theoretical curve) for drilling detritus (all particles), for milling (smaller particles) and cutting (larger particles).

It is important to observe how the internal heat production (substantially by friction) in the comminution process is included in W_{I} and W_{II}. Such quantities will be proportional to the newly produced free surface [42] and absolutely prevailing over the theoretical fracture work—only 3% of the total [1].

Evaluating the powers $\dot{W}_{\mathrm{I}}$ and $\dot{W}_{\mathrm{II}}$ by Equation (8) and $\dot{W}_{\mathrm{f}}$ as dissipated by the external friction forces, Equation (18) can be rewritten as follows:

$$F\dot{\delta} + M_{\mathrm{t}}\dot{\varphi} = \Gamma_{\mathrm{I}}^{*}\left(\frac{V_{\mathrm{I}}}{V}A_{\mathrm{bit}}\dot{\delta}\right)^{D_{\mathrm{I}}/3} + \Gamma_{\mathrm{II}}^{*}\left(\frac{V_{\mathrm{II}}}{V}A_{\mathrm{bit}}\dot{\delta}\right)^{D_{\mathrm{II}}/3} + \mu FR\dot{\varphi} \tag{19}$$

where $\Gamma_{\mathrm{I,II}}^{*}$ is the energy dissipated on the fractal free surface of the material (by fracture and internal friction) and D_{I} and D_{II} are, respectively, the fractal exponent for the primary and secondary drilling processes; A_{bit} is the effective area of the tool ring, μ the

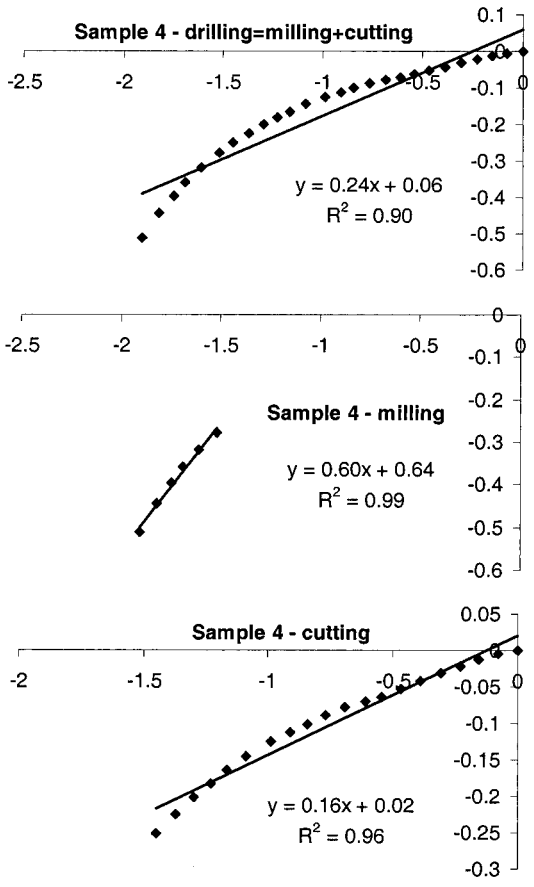

Figure 5. Sample 4—Bi-logarithmic diagrams of relative size x vs relative mass y of fragments (experimental points and theoretical curve) for drilling detritus (all particles), for milling (smaller particles) and cutting (larger particles).

friction coefficient between the two materials and R the mean radius of the drilling tool. From the experiments (Figures 2–7) it is evident that $(V_{\mathrm{I}}/V) \cong (V_{\mathrm{II}}/V) \cong \frac{1}{2}$, $D_{\mathrm{I}} \cong 2.9$, $D_{\mathrm{II}} \cong 2.1$.

Practically, it is more convenient to calculate the work dissipated in the primary comminution process putting $r_{\min} = \bar{d}/2$, $r_{\max} = d_{\max}/2$ into Equations (6) and (7), and substituting $\mathscr{G}_{\mathrm{F}}$ with $\Gamma \cong 30\mathscr{G}_{\mathrm{F}}$ (the theoretical fracture work being only 3% of the total):

$$\begin{aligned}\dot{W}_{\mathrm{I}} &\cong 15\mathscr{G}_{\mathrm{F}}\dot{A}_I = 15\mathscr{G}_{\mathrm{F}}\pi\frac{D_{\mathrm{I}}}{D_{\mathrm{I}}-2}\bar{d}^{D_{\mathrm{I}}}(\bar{d}^{2-D_{\mathrm{I}}} - d_{\max}^{2-D_{\mathrm{I}}})\dot{N}_{\mathrm{pI}} \\ &= 15\mathscr{G}_{\mathrm{F}}\pi\frac{D_{\mathrm{I}}}{D_{\mathrm{I}}-2}\bar{d}^{D_{\mathrm{I}}}(\bar{d}^{2-D_{\mathrm{I}}} - d_{\max}^{2-D_{\mathrm{I}}})\left(\frac{6}{\pi}\frac{3-D_{\mathrm{I}}}{D_{\mathrm{I}}}\frac{\dot{V}_{\mathrm{I}}}{\bar{d}^{D_{\mathrm{I}}}d_{\max}^{3-D_{\mathrm{I}}}}\right) \\ &= 60\mathscr{G}_{\mathrm{F}}\frac{3-D_{\mathrm{I}}}{D_{\mathrm{I}}-2}d_{\max}^{D_{\mathrm{I}}-3}(\bar{d}^{2-D_{\mathrm{I}}} - d_{\max}^{2-D_{\mathrm{I}}})\dot{V}_{\mathrm{I}} \end{aligned} \tag{20}$$

From the experiments we have

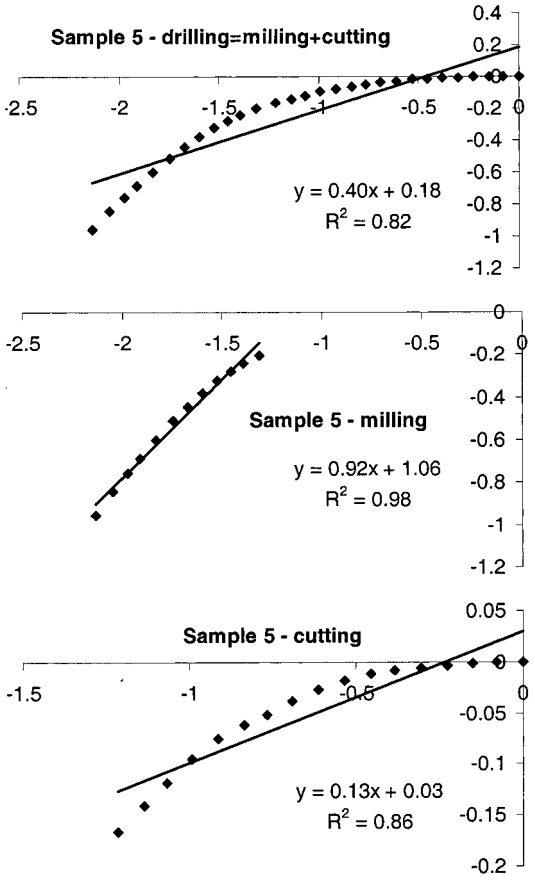

Figure 6. Sample 5—Bi-logarithmic diagrams of relative size x vs relative mass y of fragments (experimental points and theoretical curve) for drilling detritus (all particles), for milling (smaller particles) and cutting (larger particles).

$D_{\mathrm{I}} \cong 2.9$, $\dot{V}_{\mathrm{I}} \cong A_{\mathrm{bit}}\dot{\delta}/2$, $d_{\max} \cong 300\ \mu\mathrm{m}$, $\bar{d} \cong 10\ \mu\mathrm{m}$, $\mathscr{G}_{\mathrm{F}} \cong 100\ \mathrm{N/m}$, so that Equation (20) becomes

$$\dot{W}_{\mathrm{I}} \cong S_{\mathrm{I}} A_{\mathrm{bit}}\dot{\delta}, \quad S_{\mathrm{I}} \cong \sigma_{\mathrm{C}} \cong 0.03\ \mathrm{GPa} \tag{21}$$

where σ_{C} is the compressive strength of the material [49,50].

Putting $r_{\min} = d_{\min}/2$, $r_{\max} = \bar{d}/2$ in Equations (6) and (7), and substituting $\mathscr{G}_{\mathrm{F}}$ with $\Gamma \cong 30\mathscr{G}_{\mathrm{F}}$, we can obtain the work dissipated in the secondary comminution process:

$$\begin{aligned}\dot{W}_{\mathrm{II}} &\cong 15\mathscr{G}_{\mathrm{F}}\dot{A}_{\mathrm{II}} = 15\mathscr{G}_{\mathrm{F}}\pi\frac{D_{\mathrm{II}}}{D_{\mathrm{II}}-2}d_{\min}^{D_{\mathrm{II}}}(d_{\min}^{2-D_{\mathrm{II}}} - \bar{d}^{2-D_{\mathrm{II}}})\dot{N}_{\mathrm{pII}} \\ &\cong 15\mathscr{G}_{\mathrm{F}}\pi\frac{D_{\mathrm{II}}}{D_{\mathrm{II}}-2}d_{\min}^{D_{\mathrm{II}}}(d_{\min}^{2-D_{\mathrm{II}}} - \bar{d}^{2-D_{\mathrm{II}}})\left(\frac{6}{\pi}\frac{3-D_{\mathrm{II}}}{D_{\mathrm{II}}}\frac{\dot{V}_{\mathrm{II}}}{d_{\min}^{D_{\mathrm{II}}}\bar{d}_{\max}^{3-D_{\mathrm{II}}}}\right) \\ &= 60\mathscr{G}_{\mathrm{F}}\frac{3-D_{\mathrm{II}}}{D_{\mathrm{II}}-2}\bar{d}^{D_{\mathrm{II}}-3}(d_{\min}^{2-D_{\mathrm{II}}} - \bar{d}^{2-D_{\mathrm{II}}})\dot{V}_{\mathrm{II}}\end{aligned} \tag{22}$$

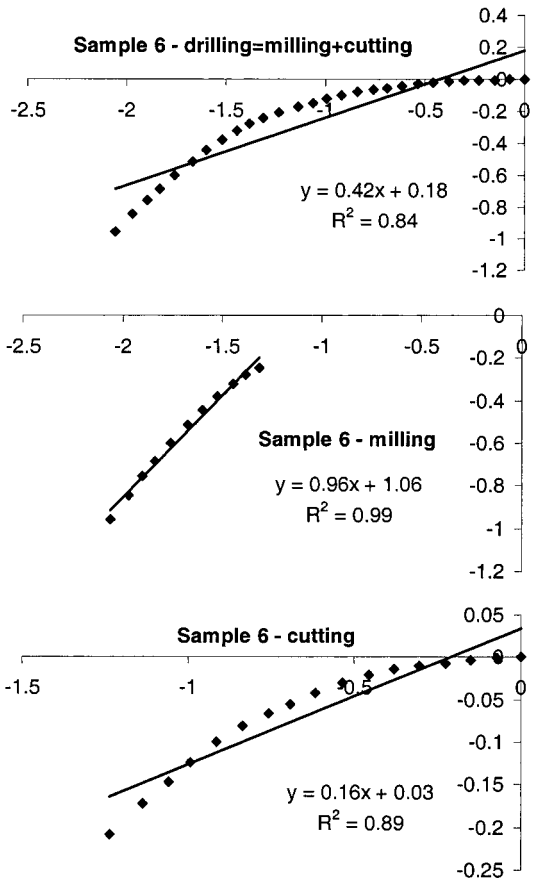

Figure 7. Sample 6—Bi-logarithmic diagrams of relative size x vs relative mass y of fragments (experimental points and theoretical curve) for drilling detritus (all particles), for milling (smaller particles) and cutting (larger particles).

From the experiments we have

$$D_{\mathrm{II}} \cong 2.1, \quad \dot{V}_{\mathrm{II}} \cong A_{\mathrm{bit}}\dot{\delta}/2, \quad d_{\min} \cong 1\ \mu\mathrm{m}, \quad \bar{d} \cong 10\ \mu\mathrm{m}, \quad \mathscr{G}_{\mathrm{F}} \cong 100\ \mathrm{N/m}$$

so that Equation (22) becomes

$$\dot{W}_{\mathrm{II}} \cong S_{\mathrm{II}} A_{\mathrm{bit}}\dot{\delta}, \quad S_{\mathrm{II}} \cong 30\sigma_{\mathrm{C}} \cong 1\ \mathrm{GPa} \tag{23}$$

Equation (19) can be consistently rewritten in the following manner:

$$F\dot{\delta} + M_{\mathrm{t}}\dot{\varphi} = (S_{\mathrm{I}} + S_{\mathrm{II}})A_{\mathrm{bit}}\dot{\delta} + \mu FR\dot{\varphi} \tag{24}$$

Since the power supplied by the operator is much smaller than the power supplied by the machine and the power consumed in the primary comminution is much smaller than the power consumed in the secondary one, we have $F\dot{\delta} \ll M_{\mathrm{t}}\dot{\varphi}$ and $\dot{W}_{\mathrm{I}} \ll \dot{W}_{\mathrm{II}}$ and Equation (24) becomes

$$M_{\mathrm{t}}\dot{\varphi} = SA_{\mathrm{bit}}\dot{\delta} + \mu FR\dot{\varphi}, \quad S \cong 30\sigma_{\mathrm{C}} \cong 1\ \mathrm{GPa} \tag{25}$$

and shows how the classical assumption $S \cong \sigma_C$ [49,50] is not correct, especially for the finer comminution for which $S \cong 30\sigma_C$.

Equation (25) can be used to describe the process from a global point of view and to predict the drilling velocity. From the experiments:

$A_{bit} = 12 \times 10^{-4}$ m^2	core bit area
$F = 250$ N	thrust
$P_{mech} = 1600$ W	ideal mechanical power supplied
$R = 5 \times 10^{-2}$ m	core bit radius
$\dot{\delta} = 0.7 \times 10^{-3}$ m/s	drilling velocity
$\mu = 0.4$	external friction coefficient
$\dot{\varphi} = 45$ rad/s	angular velocity
$\sigma_C = 0.03$ GPa	compressive strength of the material (concrete)

Introducing a machine efficiency equal to 0.9, the real mechanical power supplied to the core-bit is $M_t\dot{\varphi} = 0.9P_{mech} = 1440$ W ($\gg F\dot{\delta} = 0.175$ W). The power dissipated by the external friction is $\mu FR\dot{\varphi} = 225$ W. Equation (25) predicts a drilling velocity of $\dot{\delta} \cong 10^{-3}$ m/s which is close to an experimental value of 0.7×10^{-3} m/s.

7. CONCLUSIONS

The proposed theory emphasizes how the energy dissipation in the comminution process occurs in a fractal domain intermediate between a surface and a volume: $W \propto V^{D/3}$, $2 \leqslant D \leqslant 3$. For finer comminution the fractal exponent D is close to two, as well as for larger particles created by cutting is close to three.

The theoretical assumption of a material 'quantum' is experimentally confirmed and its characteristic dimension appears to be close to 1 μm. The experimental fragment analysis gives the characteristic fragment size of separation between primary cutting and secondary milling, of around 10 μm.

The global power balance (25) can be used to predict the drilling velocity with reasonable accuracy. It is emphasized that the drilling strength S is a not a size-independent parameter, decreasing considerably with the size scale, and that the classical assumption $S \cong \sigma_C$ is not correct, especially for the finer comminution for which $S \cong 30\sigma_C$. As a consequence, the energy dissipated on the fractal free surface Γ^*, more than the drilling strength S, can be considered as a characteristic size-independent parameter.

NOMENCLATURE

Greek letters

$\dot{\delta}$	drilling velocity
$\dot{\varphi}$	angular velocity
μ	friction coefficient between tool and base material
ρ_m	material density
σ_C	material strength

$\mathscr{G}_F$	fracture energy
$\mathscr{G}_F^*$	fractal fracture energy
Γ	dissipated energy by fracture and friction
Γ^*	fractal dissipated energy by fracture and friction

Latin letters

A	total fracture surface area of fragments
A_{bit}	core-bit area
V	fragmented volume
d	fragmented size
$\bar{d}$	fragment size of separation between cutting and milling
d_{max}	size of the largest fragment
d_{min}	size of the smallest fragment (material quantum)
D	fractal exponent
F	thrust
N_p	total number of fragments
M	total mass of fragments
$M(<r)$	mass of fragments with radius smaller than r
M_t	torque
p	probability size-distribution function for fragments
P	cumulative size-distribution function for fragments
P_{mech}	mechanical power supplied by the drilling machine
$r = d/2$	fragment radius
R	mean radius of the tool
S	drilling strength
W	energy dissipated during fragmentation
W_f	energy dissipated by external friction

Subscripts

I	primary cutting process
II	secondary milling process

ACKNOWLEDGEMENTS

The present research was carried out with the financial support of Ministry of University and Scientific Research (MIUR), National Research Council (CNR) and EC-TMR Contract No. ERBFMRXCT960062.

REFERENCES

1. Béla Beke D. *Principles of Comminution*. Publishing House of the Hungarian Academy of Sciences, 1964; 90–92.
2. Turcotte DL. *Fractals and Chaos in Geology and Geophysics*. Cambridge University Press, 1992, 20–32.
3. Mandelbrot BB. *The Fractal Geometry of Nature*. Freeman: NY, 1982.
4. Feder J. *Fractals*. Plenum Publishing Corporation: New York, 1988.
5. Grady DE, Kipp ME. Geometric statistics and dynamic fragmentation. *Journal of Applied Physics* 1985; **58**:569–583.
6. Redner S. Fragmentation. In *Statistical Models for the Fracture of Disordered Media*, Hermann HJ, Roux S (eds), Elsevier: Amsterdam, 1990; 321–348.

7. Redner S. Statistical theory of fragmentation. In *Disorder and Fracture*, Hermann HJ, Roux S, Guyon F (eds), Plenum Press: NJ, 1990; 31–48.
8. Perfect E. Fractal models for the fragmentation of rocks and soils: a review. *Engineering Geology* 1997; **48**:185–198.
9. Mishnaevsky LL. Physical mechanisms of hard rock fragmentation under mechanical loading: a review. *International Journal of Rock Mechanics and Mining Sciences & Geomechanics Abstracts* 1995; **32**:763–766.
10. Ersoy A, Waller MD. Drilling detritus and the operating parameters of thermally stable PDC core bits. *International Journal of Rock Mechanics and Mining Sciences* 1997; **34**:1109–1123.
11. Carpinteri A. Scaling laws and renormalization groups for strength and toughness of disordered materials. *International Journal of Solids and Structures* 1994; **31**:291–302.
12. Carpinteri A, Chiaia B. Multifractal scaling laws in the breaking behaviour of disordered materials. *Chaos, Solitons and Fractals* 1997; **8**:135–150.
13. Carpinteri A, Ferro G, Monetto I. Scale effects in uniaxially compressed concrete specimens. *Magazine of Concrete Research* 1999; **51**:217–225.
14. Engleman R, Rivier N, Jaeger Z. Size distribution in sudden breakage by the use of entropy maximization. *Journal of Applied Physics* 1998; **63**:4766–4768.
15. Nagahama H. Fractal fragment size distribution for brittle rocks. *International Journal of Rock Mechanics and Mining Sciences & Geomechanics Abstracts* 1993; **30**:469–471.
16. Yong Z, Hanson MT. A rotational source of plane fractals and its application to fragmentation analysis of thin plates. *Chaos, Solitons and Fractals* 1996; **7**:31–40.
17. Aharony A, Levi A, Englman R, Jaeger Z. Percolation model calculations of fragment properties. *Annual Israel Physical Society* 1986; **8**:112–119.
18. Matsushita M. Fractal viewpoint of fracture and accretion. *Journal of the Physical Society of Japan* 1985; **54**:857–860.
19. Turcotte DL. Fractal and fragmentation. *Journal of Geophysical Research* 1986; **91**:1921–1926.
20. Turcotte DL. Fractals in geology and geophysics. *Pure and Applied Geophysics* 1989; **131**:171–196.
21. Rieu M, Sposito G. Fractal fragmentation, soil porosity and soil water properties: I. Theory. *Soil Science Society of America, Journal* l991; **55**:1231–1238.
22. Crawford JW, Sleeman BD, Young JM. On the relation between number size distributions and the fractal dimension of aggregates. *Journal of Soil Science* 1993; **44**:555–565.
23. Ching ESC. Multifractality of mass distribution in fragmentation. *Physica A* 2000; **288**:402–408.
24. Sotolongo-Costa O, Rodriguez AH, Rodgers GJ. Dimensional crossover in fragmentation. *Physica A* 2000; **286**:638–642.
25. Ben-Naim E, Krapivsky PL. Fragmentation with a steady source. *Physics Letters A* 2000; **275**:48–53.
26. Sammis CG. Fractal fragmentation and frictional stability in granular materials. *IUTAM Symposium on Mechanics of Granular and Porous Materials*. Kluwer Academic Publisher: Netherlands, 1997; 23–34.
27. Hyslip P, Vallejo LE. Fractal analysis of the roughness and size distribution of granular materials. *Engineering Geology* 1997; **48**:231–244.
28. Hecht CA. Appolonian Packing and fractal shape of grains improving geomechanical properties in engineering geology. *Pure and Applied Geophysics* 2000; **157**:487–504.
29. Momber AW. The fragmentation of standard concrete cylinders under compression: the role of the secondary fracture debris. *Engineering Fracture Mechanics* 2000; **67**:445–459.
30. McDowell GR, Bolton MD, Robertson D. The fractal crushing of granular materials. *Journal of the Mechanics and Physics of Solids* 1996; **44**:2079–2102.
31. Schocke D, Arastoopour H, Bernstein B. Pulverization of rubber under high compression and shear. *Powder Technology* 1999; **102**:207–214.
32. Salman AD, Gorham DA. The fracture of glass spheres. *Powder Technology* 2000; **107**:179–185.
33. Belingardi G, Gugliotta A, Vadori A. Numerical simulation of fragmentation of composite material plates due to impact. *International Journal of Impact Engineering* 1998; **21**:335–347.
34. Ching ESC, Lui SL, Ke-Qing X. Energy dependence of impact fragmentation of long glass rods. *Physica A* 2000; **287**:83–90.
35. Tomas J, Schreier M, Gröger T, Ehlers S. Impact crushing of concrete for liberation and recycling. *Powder Technology* 1999; **105**:39–51.
36. Larsson I, Kristensen HG. Comminution of a brittle/ductile material in a Micros Ring Mill. *Powder Technology* 2000; **107**:175–178.
37. Cleary P. Modelling comminution devices using DEM. *International Journal for Numerical and Analytical Methods in Geomechanics* 2001; **25**:83–105.
38. Carpinteri A, Pugno N. Structural elements with re-entrant corners. *Proceedings of the XV National Congress of the Italian Group of Fracture*, Bari, Italy, 3–5 May 2000; 391–398.
39. Novozhilov V. On a necessary and sufficient criterion for brittle strength. *Prikladnaya Matematika i Mekhanika* 1969; **33**:212–222.
40. Carpinteri A. *Mechanical Damage and Crack Growth in Concrete*. Martinuus Nijhoff: Dordrecht, Netherlands, 1986.

41. Griffith AA. The phenomenon of rupture and flow in solids. *Philosophical Transactions of the Royal Society of London*, Series A 1921; **221**:163–198.
42. Smekal A. Physikalisches und technisches Arbeitsgesetz der Zerkleinerung. *Zeitschr*. VDI, Beiheft Verfahrenstechnik 1937; 159–161.
43. Bond FC. The third theory of comminution. *Mining Engineering* 1952; **193**:484–494.
44. Rittinger PR. *Lehrbuch der Aufbereitungskunde*. Berlin, 1867.
45. Hönig F. Grundgesetze der Zerkleinerung. *VDI Forschungsheft* 1936; **378**.
46. Kick F. *Das Gesetz der Proportionalen Widerstände*. Leipzig, 1885.
47. Stroeven P. Fractal and fractography in concrete technology. *International Symposium on Brittle Matrix Composites III*, Warsaw, Poland, 1991; 1–10.
48. Mancini R, Cardu M, Fornaro M, Linares M. Scale effects in the micro-scale rock mechanics problems. *Proceedings of the II International Workshop on Scale Effects in Rock Masses*, Lisbon, Portugal, June 25, 1993; 151–158.
49. Paone J, Bruce WE. *Drillability Studies—Diamond Drilling*. USBM-RI 6324, 1963.
50. Karanam MR, Misra B. *Principles of Rock Drilling*. Balkema: Rotterdam, 1998.

